

Ab initio computation of $d-d$ excitation energies in low-dimensional Ti and V oxychlorides

Nikolay A. Bogdanov,^{1,2} Jeroen van den Brink,¹ and Liviu Hozoi¹

¹*Institute for Theoretical Solid State Physics, IFW Dresden, Helmholtzstr. 20, 01069 Dresden, Germany*

²*National University of Science and Technology MISIS, Leninskiy pr. 4, 119049 Moscow, Russia*

(Dated: September 12, 2021)

Using a quantum chemical cluster-in-solid computational scheme, we calculate the local $d-d$ excitation energies for two strongly correlated Mott insulators, the oxychlorides TiOCl and VOCl. TiOCl harbors quasi-one-dimensional spin chains made out of $S=1/2$ Ti^{3+} ions while the electronic structure of VOCl displays a more two-dimensional character. We find in both cases that the lowest-energy $d-d$ excitations are within the t_{2g} subshell, starting at 0.34 eV and indicating that orbital degeneracies are significantly lifted. In the vanadium oxychloride, spin triplet to singlet excitations are calculated to be 1 eV higher in energy. For TiOCl, the computed d -level electronic structure and the symmetries of the wavefunctions are in very good agreement with resonant inelastic x-ray scattering results and optical absorption data. For VOCl, future resonant inelastic x-ray scattering experiments will constitute a direct test of the symmetry and energy of about a dozen of different $d-d$ excitations that we predict here.

I. INTRODUCTION

The vast majority of solid-state electronic structure calculations is based nowadays on density functional theory (DFT). For strongly correlated systems, however, the wavefunction based *ab initio* methods certainly provide a viable alternative. For this class of materials, of which a typical example are the parent compounds of the high- T_c copper oxide superconductors, it is essential to properly describe the multiconfigurational character of the many-electron wavefunction. The multiconfiguration and multi-reference quantum chemical methods constitute here a natural choice. When i) the clusters on which such computational techniques are applied are large enough and ii) the embedding potential describing the crystalline surroundings is judiciously constructed, the wavefunction based approach yields results in excellent agreement with the experimental data. This has been recently shown for the sequence of spin-state transitions in a d^6 system, LaCoO_3 ,¹ and the d -orbital electronic structure of a number of Cu d^9 oxides.² We used in those studies a fully *ab initio* embedding scheme in which the effective embedding potential is constructed on the basis of prior periodic Hartree-Fock (HF) calculations for the extended crystal, in contrast to other quantum chemical investigations based on simpler point charge embeddings.³ Further, as a general recipe, the embedded cluster that enters the post-HF treatment comprises in our approach in addition to the “central” MO_6 octahedron the nearest-neighbor (NN) octahedra, where M is a transition-metal ion. The finite charge distribution of the NN octahedra and the tails of “central” Wannier orbitals extending to neighboring sites are thus described with high accuracy. For the particular case of $d-d$ excitation energies in Cu d^9 oxides,² excellent agreement was found with state of the art resonant inelastic x-ray scattering (RIXS) experiments.⁴ Yet, as compared to earlier quantum chemical calculations on smaller single-octahedron

$[\text{CuO}_6]$ clusters embedded in arrays of point charges,⁵ differences as large as 0.5 eV were observed.²

In the present work, we verify the performance of our cluster-in-solid computational scheme for the case of low-dimensional Ti d^1 and V d^2 Mott insulators, in particular, the TiOCl and VOCl compounds. The d -level electronic structure of TiOCl has been previously addressed by optical absorption experiments corroborated with model Hamiltonian configuration-interaction (CI) simulations of the optical spectra,^{6,7} DFT-based investigations,⁸⁻¹¹ *ab initio* quantum chemical cluster calculations,¹² and RIXS measurements.¹³ The V oxychloride compound, on the other hand, is much less investigated. On the experimental side, basic information concerning its d -level electronic structure is available from optical absorption data.¹⁴ Here, we perform a detailed quantum chemical investigation to better understand the nature and symmetry of the different excited states identified by optical experiments.¹⁴

II. STRUCTURAL AND COMPUTATIONAL DETAILS

TiOCl and VOCl display the same highly anisotropic crystalline structure, with a bilayer network of metal and oxygen sites well separated along the crystallographic c axis by double Cl layers (see Fig. 1). Each metal ion lies in the center of a distorted O_4Cl_2 octahedron. Adjacent octahedra share edges along the b axis and corners along a . The unit cell is orthorhombic, with space group $Pm\bar{m}n$ (number 59).^{15,16}

Our computational investigation implies a sequence of several steps. Periodic restricted HF calculations are first performed with the CRYSTAL package.¹⁷ We used the experimental lattice parameters and all-electron Gaussian-type basis sets. Further post-HF correlation calculations are carried out on finite embedded clusters. The same type of cluster is employed for both TiOCl and VOCl.

It consists of nine MO_4Cl_2 octahedra, i.e., one reference octahedron plus eight neighboring octahedra, where M is either Ti or V. The reference octahedron in the center of this cluster \mathcal{C} defines the active region \mathcal{C}_A where local $d-d$ excitations are explicitly computed. The adjacent eight octahedra constitute a buffer region \mathcal{C}_B . The role of the sites in \mathcal{C}_B is to provide support for the tails of Wannier orbitals (WO's) in the \mathcal{C}_A region.

The orbital basis for the correlation calculations is a set of projected HF Wannier functions. Localized HF WO's are obtained with the Wannier-Boys localization module¹⁸ of the CRYSTAL package and subsequently projected onto the set of Gaussian basis functions associated with the atomic sites of the cluster \mathcal{C} . For our choice of \mathcal{C}_B , the norms of the projected WO's centered within the active region \mathcal{C}_A are not lower than 99.8% of the original HF WO's. Additionally, the HF data is used to generate an effective embedding potential for the nine-octahedra fragment \mathcal{C} . This potential is obtained from the Fock operator in the restricted HF calculation and models the surroundings of the finite cluster, i.e., the remaining of the crystalline lattice.

While the doubly occupied WO's in the buffer region \mathcal{C}_B are kept frozen, all valence orbitals centered at ligand and metal sites in \mathcal{C}_A (and their tails in \mathcal{C}_B) are further re-optimized in multiconfiguration complete-active-space self-consistent-field (CASSCF) calculations. In the latter, the ground-state wavefunction and the crystal-field excited states at the central Ti/V site are computed in state-averaged multiroot calculations. The d -level splittings are finally obtained by additional single and double CI (MRCI) calculation.¹⁹ The whole procedure is described in more detail in Ref. 2.

The CASSCF and MRCI investigations are carried out with the MOLPRO package.²⁰ The effective embedding potential is added to the one-electron Hamiltonian in the CASSCF/MRCI computations with the help of the CRYSTAL-MOLPRO interface.²¹

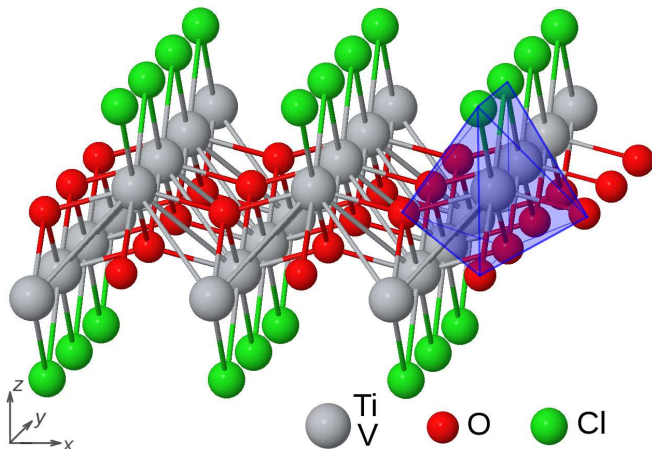


FIG. 1. Layered crystal structure of TiOCl and VOCl. A distorted O_4Cl_2 octahedron is highlighted on the right hand side.

TABLE I. Ti^{3+} d -level splittings in TiOCl. A non-standard local reference system is chosen for the octahedrally coordinated Ti ion, see Fig. 1, with a rotation of 45° around x . The ground-state $d_{y^2-z^2}^1$ configuration is taken as reference. All energies are given in eV.

| Orbital occupation | CASSCF/MRCI | CASSCF/CASPT2 ^a |
|--------------------|-------------|----------------------------|
| $d_{y^2-z^2}^1$ | 0/0 | 0/0 |
| d_{xy}^1 | 0.36/0.34 | 0.29/0.29 |
| d_{xz}^1 | 0.65/0.63 | 0.66/0.68 |
| d_{yz}^1 | 1.51/1.55 | 1.59/1.68 |
| $d_{x^2}^1$ | 2.35/2.36 | 2.30/2.37 |

^a Ref. 12.

We used O and Cl basis sets of triple-zeta quality as designed by Towler *et al.*²² and Prencipe *et al.*²³ For the Ti^{3+} and V^{3+} species, we employed the triple-zeta s and p basis sets of Mackrodt *et al.*²⁴ and Dovesi *et al.*²⁵, respectively, plus triple-zeta d basis functions as designed by Ahlrichs *et al.*²⁶

III. RESULTS AND DISCUSSION

A. TiOCl

The magnetic properties of TiOCl have been the topic of extensive investigations over the last decade. The largest intersite interactions are antiferromagnetic (AF), occur between NN Ti^{3+} $S = 1/2$ sites along the b axis, and give rise to AF spin chains along that direction. The interchain couplings are also sizable and responsible for geometrical frustration.

The doubling of the unit cell in the low-temperature nonmagnetic phase^{27,28} suggests a spin-Peierls dimerized ground state at low temperatures. The observed deviations from conventional spin-Peierls behavior, e.g., the existence of two distinct phase transitions at 91 and 67 K, were attributed to the above mentioned frustration of the interchain interactions.⁶

As concerns the electronic structure of TiOCl, DFT calculations within the local density approximation (LDA) indicate sizable occupation numbers for each of the Ti t_{2g} levels.⁸⁻¹¹ Early interpretations of the unusual physical properties of this material thus invoked the presence of strong orbital fluctuations.^{8,9,29} Inclusion of local Mott-Hubbard type correlations within dynamical mean-field theory (DMFT) and LDA+DMFT calculations effectively pulls one of the t_{2g} levels below the other two components and reduces the occupation of the latter to nearly 0.^{10,11} On the theoretical side, this is confirmed by earlier quantum chemical cluster calculations¹² as well by our present results.

In Table I, CASSCF and MRCI results for TiOCl are listed. The active orbital set contains all five $3d$ functions at the central Ti site and the singly occupied $3d_{y^2-z^2}$ or-

bitals at the eight Ti NN sites. We considered high-spin intersite couplings, i.e., a ferromagnetic (FM) configuration of Ti d spins. Although the WO's at the atomic sites of \mathcal{C} are derived from periodic restricted HF calculations for the Ti $3d^1$ electron configuration, the embedding potential is obtained by replacing the $\text{Ti}^{2+} 3d^1$ ions by closed-shell $\text{V}^{2+} 3d^2$ species. This is a good approximation for the farther $3d$ -metal sites, as the comparison between our results and RIXS data shows. An extension of our embedding scheme toward the construction of open-shell embeddings is planned for the near future. In addition to the active Ti $3d$ functions in \mathcal{C}_A and \mathcal{C}_B , all O $2p$ and Cl $3p$ orbitals at the central octahedron are included in the CISD calculations.

As expected for a d^1 system, the MRCI treatment brings minor corrections to the d - d CASSCF excitation energies. Our results are compared in Table I with earlier CASSCF and CASPT2 (complete-active-space second-order perturbation theory) data from Ref. 12. A major difference between the present and earlier quantum chemical calculations is the size of the embedded clusters, i.e., nine octahedra here and one octahedron in Ref. 12. In contrast to other systems, e.g., layered Cu d^9 oxides such as La_2CuO_4 and $\text{Sr}_2\text{CuO}_2\text{Cl}_2$ where differences of about 0.5 eV were found as function of the cluster size (see the discussion in Ref. 2), the agreement between the two sets of results is good for TiOCl .

Good agreement is also found with RIXS and optical absorption experimental data, with deviations not larger than 0.1 eV. The only exception is the $d_{y^2-z^2}$ to d_{x^2} excitation, which is predicted to occur at 2.36 eV in the quantum chemical calculations and observed at about 2 eV in RIXS, see Table II. In the optical absorption measurements,^{6,7} this particular transition as well as the $d_{y^2-z^2}$ to d_{xy} excitation were not identified, which is related to the different selection rules for RIXS and optical absorption.

We recall at this point that in a first approximation the total energy of a given state within the d^n manifold is a sum of a crystal-field contribution, i.e., an on-site crystal-field splitting, and a magnetic term (see also the discussion in Refs. 2 and 4). For the ground-state con-

figuration of TiOCl , the NN spin interactions along Ti chains parallel to the b axis are quite large, $J_b \approx 57$ meV,⁸ and AF. From the exact Bethe-ansatz solution of the one-dimensional Heisenberg Hamiltonian,³⁰ the AF ground-state stabilization energy is $J \ln 2$. On the other hand, from overlap considerations, the (super)exchange with the NN Ti $d_{y^2-z^2}$ spins is either zero or much weaker for the crystal-field excited states. Since the quantum chemical calculations were performed for a FM cluster,³¹ for a meaningful comparison between the MRCI and RIXS data, we subtracted in Table II from the relative RIXS energies reported in Ref. 13 a term $J_b \ln 2 \approx 0.04$ eV representing the energy stabilization of the AF ground-state with respect to the crystal-field excited states.

B. VOCl

In the family of correlated transition-metal oxide materials, the vanadium compounds display an impressive variety of vanadium valence states, crystalline structures, and physical properties. The valence configuration, for example, may vary from $\text{V}^{2+} d^3$ in VO_{1-x} ^{32,33} to $\text{V}^{4+} d^1$ in CaV_2O_5 ³⁴ and NaV_2O_5 .³⁵ While the latter vanadates display a layered lattice with ladders of O-bridged V sites, VO_{1-x} has a rocksalt crystalline structure. At the level of *ab initio* wavefunction calculations, the V oxides are rather unexplored. To our knowledge, only the ladder vanadates have been investigated by advanced quantum calculations.³⁴⁻³⁶

Besides having two electrons instead of one within the t_{2g} set of orbitals, VOCl also displays in comparison to TiOCl a more pronounced two-dimensional character as concerns the electronic structure and magnetic properties.³⁷ In Table III, V d - d excitation energies for the VOCl compound are given. Two different sets of CASSCF calculations were carried out, for two different electron configurations at each of the V NN's. Preliminary CASSCF calculations were first performed with eighteen orbitals in the active space, i.e., two t_{2g} orbitals at each of the V sites in the nine-octahedra cluster. As for TiOCl , we considered high-spin intersite couplings, i.e., a FM cluster. It turns out that the dominant ground-state configuration at a given V site is $d_{y^2-z^2}^1 d_{xy}^1$. The crystal-field excited states for the central V ion are then obtained in state-averaged multiroot computations where a group of three additional orbitals was added to the active space. To be sure that the three additional orbitals are localized at the central V site and to allow only for on-site d - d excitations, the occupation of the NN $d_{y^2-z^2}$ and d_{xy} functions was restricted to 1. Crystal-field splittings obtained from such SCF calculations are listed in the third column of Table III. To avoid complications related to states that display low-spin intersite couplings, only the high-spin on-site excitations were computed in this case.

We note that the ground-state electron configuration in the periodic restricted HF calculation is $d_{y^2-z^2}^1 d_{xy}^1$ but

TABLE II. Ti d - d excitation energies in TiOCl , quantum chemical vs. experimental results. A $J_b \ln 2$ term was here subtracted from each of the RIXS values reported in Ref. 13, see text. All energies are given in eV.

| Orbital occupation | MRCI | RIXS ^a | Optics ^b |
|--------------------|------|-------------------|---------------------|
| $d_{y^2-z^2}^1$ | 0 | 0 | 0 |
| d_{xy}^1 | 0.34 | 0.32 | — |
| d_{xz}^1 | 0.63 | 0.55 | 0.65 |
| d_{yz}^1 | 1.55 | 1.41 | 1.50 |
| $d_{x^2}^1$ | 2.36 | 2.01 | — |

^a Ref. 13.

^b Ref. 7.

TABLE III. V $d-d$ excitation energies in VOCl. A non-standard local reference system is chosen, see Fig. 1, with a rotation of 45° around x . The dominant ground-state configuration is $d_{y^2-z^2}^1 d_{xy}^1$, with a weight of 81%. For each of the excited states, the weight of the dominant configuration is not smaller than 64%. All energies are given in eV.

| Dominant configuration | CASSCF ^a | CASSCF ^b | MRCI ^b | Optics ^c |
|------------------------|---------------------------|---------------------|-------------------|---------------------|
| $t_{2g}^2, S=1$ | $d_{y^2-z^2}^1 d_{xy}^1$ | 0 | 0 | 0 |
| | $d_{y^2-z^2}^1 d_{xz}^1$ | 0.36 | 0.36 | 0.34 |
| | $d_{xy}^1 d_{xz}^1$ | 0.43 | 0.44 | 0.46 |
| $t_{2g}^1 e_g^1, S=1$ | $d_{xy}^1 d_{yz}^1$ | 1.61 | 1.60 | 1.73 |
| | $d_{y^2-z^2}^1 d_{x^2}^1$ | 1.74 | 1.71 | 1.82 |
| | $d_{xz}^1 d_{yz}^1$ | 1.75 | 1.73 | 1.88 |
| | $d_{y^2-z^2}^1 d_{yz}^1$ | 2.85 | 2.82 | 2.55 |
| | $d_{xz}^1 d_{x^2}^1$ | 3.53 | 3.52 | 3.17 |
| | $d_{xy}^1 d_{x^2}^1$ | 3.53 | 3.53 | 3.19 |
| $t_{2g}^2, S=0$ | $d_{y^2-z^2}^2$ | | 1.27 | 1.47 |
| | $d_{y^2-z^2}^1 d_{xy}^1$ | | 1.28 | 1.47 |
| | $d_{y^2-z^2}^1 d_{xz}^1$ | | 1.56 | 1.75 |
| | d_{xz}^2 | | 1.79 | 1.97 |
| | $d_{xy}^1 d_{xz}^1$ | | 1.81 | 2.00 |

^a High-spin V $d_{y^2-z^2}^1 d_{xy}^1$ NN's, see text.

^b Closed-shell V $d_{y^2-z^2}^2$ NN's.

^c Ref. 14.

in the construction of the HF embedding potential we imposed a closed-shell V $d_{y^2-z^2}^2$ configuration for the remaining part of the lattice. In a second set of CASSCF calculations, we imposed a closed-shell $d_{y^2-z^2}^2$ electron configuration for the V NN's in the C_B region of the cluster as well. Minor variations were found as compared to the CASSCF $d-d$ excitation energies with high-spin $d_{y^2-z^2}^1 d_{xy}^1$ NN's, i.e., less than 0.01 eV for the lowest three roots and less than 0.03 eV for the higher roots. The CASSCF V crystal-field splittings for closed-shell V NN's are given in the fourth column of Table III. The latter CASSCF wavefunctions were used as reference wavefunctions in further MRCI calculations. Those MRCI results are listed in the fifth column of Table III. Only the V $3d$, O $2p$, and Cl $3p$ orbitals at the central octahedron were correlated in the MRCI treatment.

The agreement between our quantum chemical data and optical absorption results reported in Ref. 14 is very good, especially for the lowest two excitations (see Table III). The small difference between those excitation energies indicates that the splitting between the $d_{y^2-z^2}$ and d_{xy} levels, singly occupied in the ground-state configuration, is also small, about 0.1 eV. On the other hand, the energy separation between the d_{xy} and d_{xz} levels is substantially larger, 0.3 eV, and indicates that orbital fluctuations are unlikely to be important in VOCl. As concerns the $S=0$ singlet excitations, they acquire very low intensity in the optical spectra. On the experimental side, a better characterization of those states call for high-resolution RIXS measurements.

IV. CONCLUSIONS

With a quantum chemical cluster-in-solid computational scheme, we have determined the $d-d$ excitation energies of TiOCl and VOCl. The ground state configuration is t_{2g}^1 for Ti and high-spin t_{2g}^2 for V. The lowest-energy $d-d$ excitations are for both materials within the t_{2g} subshell, starting at 0.34 eV. We conclude that therefore orbital degeneracies are lifted to a similar and significant extent in the two systems, which excludes the presence of strong orbital fluctuations in the ground state. In the vanadium oxychloride, spin triplet to singlet excitations start at an excitation energy of 1.47 eV and above. The computed d -level electronic structure and the symmetries of the wavefunctions are in very good agreement with RIXS results and optical absorption data for TiOCl. For VOCl, future RIXS experiments will constitute a direct and stringent test of the symmetry and energy of about a dozen of different $d-d$ excitations that we predict here.

ACKNOWLEDGMENTS

We thank L. Siurakshina, J. Geck, R. Claessen, and M. Grüninger for useful discussions. N. B. acknowledges financial support from the Erasmus Mundus Programme of the European Union. L. H. acknowledges financial support from the German Research Foundation (Deutsche Forschungsgemeinschaft, DFG).

- ¹ L. Hozoi, U. Birkenheuer, H. Stoll, and P. Fulde, *New J. Phys.* **11**, 023023 (2009).
- ² L. Hozoi, L. Siurakshina, P. Fulde, and J. van den Brink, *Sci. Rep.* **1**, 65 (2011).
- ³ For the description of point-charge embedding techniques, see, e.g., 38–42 and Refs. therein. Hartree-Fock embeddings are also used for weakly correlated materials by Shukla *et al.*⁴³. For the construction of DFT embeddings, we refer to Refs. 44–48. The use of DFT embedding techniques for wavefunction cluster calculations in correlated 3d-metal oxides is rather scarce. Frozen DFT embeddings can easily be constructed with our present computational scheme too.
- ⁴ L. J. P. Ament, M. van Veenendaal, T. P. Devereaux, J. P. Hill, and J. van den Brink, *Rev. Mod. Phys.* **83**, 705 (2011).
- ⁵ C. de Graaf and R. Broer, *Phys. Rev. B* **62**, 702 (2000).
- ⁶ R. Rückkamp, J. Baier, M. Kriener, M. W. Haverkort, T. Lorenz, G. S. Uhrig, L. Jongen, A. Möller, G. Meyer, and M. Grüninger, *Phys. Rev. Lett.* **95**, 097203 (2005).
- ⁷ R. Rückkamp, E. Benckiser, M. W. Haverkort, H. Roth, T. Lorenz, A. Freimuth, L. Jongen, A. Müller, G. Meyer, P. Reutler, B. Büchner, A. Revcolevschi, S.-W. Cheong, C. Sekar, G. Krabbes, and M. Grüninger, *New J. Phys.* **7**, 144 (2005).
- ⁸ A. Seidel, C. A. Marianetti, F. C. Chou, G. Ceder, and P. A. Lee, *Phys. Rev. B* **67**, 020405 (2003).
- ⁹ T. Saha-Dasgupta, R. Valentí, H. Rosner, and C. Gros, *Europhys. Lett.* **67**, 63 (2004).
- ¹⁰ T. Saha-Dasgupta, A. Lichtenstein, and R. Valentí, *Phys. Rev. B* **71**, 153108 (2005).
- ¹¹ L. Craco, M. S. Laad, and E. Müller-Hartmann, *J. Phys.: Condens. Matter* **18**, 10943 (2006).
- ¹² D. Fausti, T. T. A. Lummen, C. Angelescu, R. Mavoz, J. Luzon, R. Broer, P. Rudolf, P. H. M. van Loosdrecht, N. Tristan, B. Büchner, S. van Smaalen, A. Möller, G. Meyer, and T. Taetz, *Phys. Rev. B* **75**, 245114 (2007).
- ¹³ S. Glawion, J. Heidler, M. W. Haverkort, L. C. Duda, T. Schmitt, V. N. Strocov, C. Monney, K. J. Zhou, A. Ruff, M. Sing, and R. Claessen, *Phys. Rev. Lett.* **107**, 107402 (2011).
- ¹⁴ E. Benckiser, R. Rückkamp, T. Möller, T. Taetz, A. Möller, A. A. Nugroho, T. T. M. Palstra, G. S. Uhrig, and M. Grüninger, *New J. Phys.* **10**, 053027 (2008).
- ¹⁵ E. M. Snigireva, S. I. Troyanov, and V. B. Rybakov, *Zh. Neorg. Khim.* **35**, 1108 (1990).
- ¹⁶ A. Haase and G. Brauer, *Acta Crystallogr. B* **31**, 2521 (1975).
- ¹⁷ CRYSTAL 2000, University of Torino, Italy.
- ¹⁸ C. M. Zicovich-Wilson, R. Dovesi, and V. R. Saunders, *J. Chem. Phys.* **115**, 9708 (2001).
- ¹⁹ For a monograph, see T. Helgaker, P. Jørgensen, and J. Olsen, *Molecular Electronic-Structure Theory* (Wiley, Chichester, 2000).
- ²⁰ MOLPRO 2006, Cardiff University, United Kingdom.
- ²¹ CRYSTAL-MOLPRO interface, Max-Planck-Institut für Physik Komplexer Systeme Dresden, Germany.
- ²² M. D. Towler, N. M. Harrison, and M. I. McCarthy, *Phys. Rev. B* **52**, 5375 (1995).
- ²³ M. Prencipe, A. Zupan, R. Dovesi, E. Aprà, and V. R. Saunders, *Phys. Rev. B* **51**, 3391 (1995).
- ²⁴ W. C. Mackrodt, E. A. Simson, and N. M. Harrison, *Surf. Sci.* **384**, 192 (1997).
- ²⁵ M. Catti, G. Sandrone, and R. Dovesi, *Phys. Rev. B* **55**, 16122 (1997).
- ²⁶ A. Schäfer, H. Horn, and R. Ahlrichs, *J. Chem. Phys.* **97**, 2571 (1992).
- ²⁷ M. Shaz, S. van Smaalen, L. Palatinus, M. Hoinkis, M. Klemm, S. Horn, and R. Claessen, *Phys. Rev. B* **71**, 100405 (2005).
- ²⁸ T. Sasaki, T. Nagai, K. Kato, M. Mizumaki, T. Asaka, M. Takata, Y. Matsui, H. Sawa, and J. Akimitsu, *Sci. Technol. Adv. Mater.* **7**, 17 (2006).
- ²⁹ P. Lemmens, K. Y. Choi, G. Caimi, L. Degiorgi, N. N. Kovaleva, A. Seidel, and F. C. Chou, *Phys. Rev. B* **70**, 134429 (2004).
- ³⁰ L. Hulthén, *Ark. Mat. Astr. Fys.* **1**, 26A (1938).
- ³¹ The virtual orbital space in the MRCI calculations cannot be presently restricted just to the \mathcal{C}_A region. It thus includes virtual orbitals in both \mathcal{C}_A and \mathcal{C}_B , which leads to very large MRCI expansions, $\sim 10^{10}$ Slater determinants for the nine-octahedra FM cluster. For practical reasons, we thus restrict the MRCI calculations to FM alignment of the Ti d spins.
- ³² M. D. Banus, T. B. Reed, and A. J. Strauss, *Phys. Rev. B* **5**, 2775 (1972).
- ³³ A. D. Rata, V. Kataev, D. Khomskii, and T. Hibma, *Phys. Rev. B* **68**, 220403 (2003).
- ³⁴ C. de Graaf, L. Hozoi, and R. Broer, *J. Chem. Phys.* **120**, 961 (2004).
- ³⁵ L. Hozoi, A. H. de Vries, A. B. van Oosten, R. Broer, J. Cabrero, and C. de Graaf, *Phys. Rev. Lett.* **89**, 076407 (2002).
- ³⁶ N. Suaud and M.-B. Lepetit, *Phys. Rev. Lett.* **88**, 056405 (2002).
- ³⁷ A. Wiedenmann, J. P. Venien, P. Palvadeau, and J. Rossat-Mignod, *J. Phys. C: Solid State Phys.* **16**, 5339 (1983).
- ³⁸ A. Sadoc, C. de Graaf, and R. Broer, in *Encyclopedia of Materials: Science and Technology*, edited by K. H. J. Buschow, R. W. Cahn, M. C. Flemings, B. Ilshner, E. J. Kramer, S. Mahajan, and P. Veysiere (Elsevier, Oxford, 2008) pp. 1–6.
- ³⁹ M.-B. Lepetit, N. Suaud, A. Gelle, and V. Robert, *J. Chem. Phys.* **118**, 3966 (2003).
- ⁴⁰ C. Müller and K. Hermansson, *Surf. Sci.* **603**, 3329 (2009).
- ⁴¹ B. Paulus, *Phys. Rep.* **428**, 1 (2006).
- ⁴² O. Danyliv, L. Kantorovich, and F. Corá, *Phys. Rev. B* **76**, 045107 (2007).
- ⁴³ A. Shukla, M. Dolg, P. Fulde, and H. Stoll, *Phys. Rev. B* **57**, 1471 (1998).
- ⁴⁴ C. Huang, M. Pavone, and E. A. Carter, *J. Chem. Phys.* **134**, 154110 (2011).
- ⁴⁵ S. Fux, C. R. Jacob, J. Neugebauer, L. Visscher, and M. Reiher, *J. Chem. Phys.* **132**, 164101 (2010).
- ⁴⁶ O. Roncero, M. P. de Lara-Castells, P. Villarreal, F. Flores, J. Ortega, M. Paniagua, and A. Aguado, *J. Chem. Phys.* **129**, 184104 (2008).
- ⁴⁷ I. V. Abarenkov, M. A. Boyko, and P. V. Sushko, *Int. J. Quantum Chem.* **111**, 2602 (2011).

⁴⁸ J. D. Goodpaster, N. Ananth, F. R. Manby, and I. T. F. Miller, *J. Chem. Phys.* **133**, 084103 (2010).